Iranian Journal of Chemical Engineering

Journal Homepage: www.ijche.com

pISSN: 1735-5397
eISSN: 2008-2355

Dual-Functional PVC/MWCNT Nanocomposite Ion-Exchange Membranes for Water Desalination and Chemical Production

Mohammad Mahdi Behvand Usefi [1], Mohsen Mohsennia [2]*, Mehdi Sedighi [3]

[1] Department of Chemical Engineering, University of Kashan, Kashan, Iran
[2] Thermodynamic Research Laboratory, University of Kashan, Kashan, Iran
[3] Department of Chemical Engineering, University of Qom, Qom, Iran

ARTICLE INFO

Article type:
Research article

Article history:
Received: 2026-02-04
Revised: 2026-03-04
Accepted: 2026-03-22
Available online: 2026-03-25

Keywords:
PVC/MWCNTs composite,
Ion-exchange membrane,
Electrodialysis metathesis,
Desalination eficinecy,
Ion selectivity

ABSTRACT

This study investigates the performance of an electrodialysis metathesis (EDM) process using polyvinyl chloride/carbon nanotube (PVC/MWCNTs) nanocomposite ion-exchange membranes (IEMs) for simultaneous water desalination and chemical production. IEMs, with MWCNTs loadings of 0% (M1), 4% (M2), 8% (M3), and 10% (M4) by weight, were fabricated and characterized for water sorption, areal electrical resistance, hydrophobicity, and mechanical strength. Their ion selectivity, separation performance, desalination efficiency, and production yield were systematically evaluated under varying applied voltages, feed compositions, and operation times. Among the fabricated membranes, M3 (8 wt% MWCNTs) exhibited the best performance, providing optimal ionic conductivity, selectivity, and structural stability. The maximum chemical yield was achieved when the solute concentrations in the electrode chambers exceeded those in the desalination chamber. In contrast, M4 (10 wt% MWCNTs) showed reduced efficiency, attributed to the agglomeration of MWCNTs and pore blockage that hindered ion transport. Increasing voltage improved ion transport to the optimal level, but excessive voltage (15 V) caused water splitting and concentration polarization, lowering both chemical yield and desalination efficiency. These results highlight the importance of optimizing MWCNT loading and controlled operating conditions. Overall, PVC/MWCNT composite IEMs exhibited significant potential for integrated chemical production and the treatment of saline wastewater, providing a cost-effective and scalable strategy for resource recovery.

DOI: 10.22034/ijche.2026.573395.1585 URL: https://www.ijche.com/article_244452.html

*Corresponding author: m.mohsennia@kashanu.ac.ir

1. Introduction

Advances in science and technology have profoundly transformed human social life, while simultaneously contributing to environmental pollution. Addressing these challenges necessitates effective pollution control and the development of innovative green industrial processes and products [1]. Water is an essential resource for human societies. However, natural water sources have increasingly been contaminated by anthropogenic activities. Major pollutants include sewage and industrial effluents such as dyes, pesticides, oils, heavy metals, and various inorganic and organic compounds. This contamination poses serious risks to environmental and public health and results in significant economic consequences. To address these challenges, the production of freshwater through desalination technologies has been proposed [2-4]. Among Various desalination techniques, membrane-based processes such as reverse osmosis (RO) and electrodialysis (ED) are the most commonly applied methods for both desalination and ion separation [5-8]. ED, using homogeneous or heterogeneous ion-exchange membranes (IEMs), continues to attract significant interest due to its high efficiency in water recovery, operational robustness, adaptability, and energy-saving potential [9-13]. Various strategies, including polymer selection, polymer blending, surface modification, and incorporation of nanomaterials, have been explored to enhance membrane performance, [14-16]. Nanomaterials have been employed to improve membrane flux, selectivity, and chemical and mechanical stability [17-20]. Specifically, nanocomposite membranes that combine polymers with nanomaterials, such as carbon nanotubes (CNTs), have shown promise due to the unique properties of CNTs, including high mechanical strength, purity, cost-effectiveness, and scalability [21-25]. More recently, electrodialysis metathesis (EDM) has emerged as an advanced variant of conventional ED, utilizing standard CEMs and AEMs. EDM offers several advantages, including lower energy consumption, higher product purity, and reduced post-treatment requirements [26-28]. The technique has been applied to produce high-value potassium salts [29].

Despite these advances, ongoing research has focused on the development of nanocomposite IEMs based on diverse polymer matrices and nanostructured fillers to further enhance membrane performance in terms of physicochemical, electrochemical, and transport properties, including ion conductivity, selectivity, hydrophilicity, mechanical strength, and fouling resistance. From a practical implementation perspective, the choice of materials is also strongly influenced by economic and scalability considerations. Accordingly, cost-effectiveness remains a critical factor in the selection of polymer matrices for large-scale applications. In this regard, polyvinyl chloride (PVC), a low-cost polymer, is widely considered a promising candidate due to its favorable combination of chemical stability, mechanical robustness, and economic feasibility.

Although PVC/multiwalled carbon nanotube (MWCNT) nanocomposite membranes have been extensively investigated in electrodialysis and related separation processes, their application in EDM remains scarcely reported in the literature. PVC/MWCNT-based heterogeneous IEMs have been successfully developed and evaluated for ion transport and desalination applications, demonstrating improved electrochemical performance compared to unmodified membranes. For instance, PVC/MWCNT mixed-matrix heterogeneous IEMs have been fabricated and shown to

enhance ionic flux and reduce electrical resistance during electrodialysis processes, thereby improving the transport of mono- and divalent ions in aqueous systems [30]. Similarly, PVC-based nanocomposite IEMs, containing CNTs and metal nanolayers, have exhibited improved selectivity, flux behavior, and mechanical stability in desalination applications [31]. In addition, PVC-based heterogeneous IEMs, modified with MWCNT-containing nanofillers, have demonstrated enhanced water transport properties and reduced membrane resistance, confirming the beneficial role incorporating MWCNT to improve membrane electrochemical characteristics [32]. More broadly, CNT-reinforced polymeric membranes have been reported to significantly enhance permeability, antifouling resistance, and ion transport efficiency in water treatment and separation technologies [33]. Despite these advances, no specific studies have yet systematically addressed the integration of PVC/MWCNT nanocomposite IEMs within EDM systems, indicating a clear research gap and potential for further investigation.

The present study investigates the application of the EDM process for the dual purposes of water desalination and potassium glutamate (PG) synthesis, thereby proposing an effective and cost-efficient strategy to simultaneously address water purification and resource recovery. The work specifically evaluates the performance of an EDM system employing PVC-based IEMs modified with varying concentrations of MWCNTs to enhance their structural and functional properties. Initially, the fabricated IEMs were characterized in terms of water sorption, areal electrical resistance, hydrophobicity, and mechanical strength. To systematically assess the system performance, several key operational parameters, including the initial feed concentration in the cathode, desalination, and anode compartments, as well as the applied voltage and operation time, were critically analyzed to determine their influence on both the desalination efficiency and the yield of target chemical products. The results of this study provide new insights into the design and optimization of EDM systems, highlighting their potential as sustainable and cost-effective platforms for integrated water treatment and the production of value-added chemicals.

2. Experimental

2.1. Materials

All chemical reagents used in this study were obtained from Merck & Co (Germany). Sodium chloride (NaCl) and potassium chloride (KCl) were introduced into the cathode and anode chambers respectively, while sodium gluconate (SG) was utilized in the desalination chamber. Tetrahydrofuran (THF, analytical grade), medical-grade PVC (pore size: 50 μm, porosity: 80%, wettability: hydrophobic), strongly basic anion exchange resin (Amberlite IRA-410) and strongly acidic cation exchanger (Amberlyst® 15) were used for the fabrications of IEMs. MWCNT (purity: >0.95, outside diameter: 20-30 nm, inside diameter: 5-10 nm, length : 10-30 μm) was obtained from US Research Nanomaterials, Inc. To maintain solution purity and eliminate the risk of contamination, deionized water (DI) was used to prepare all experimental solutions.

2.2. Instruments

A state-of-the-art membrane applicator was employed to fabricate IEMs, ensuring high uniformity and fabrication quality. To monitor the ionic behavior within the anode, cathode, and desalination chambers, a total dissolved solids (TDS) meter (EZDO 6031) was utilized, providing the real-time and accurate measurements of the concentrations of ions throughout the experimental trials. The system performance was monitored using several

analytical tools: electrical current fluctuations were tracked with a digital multimeter (DEC330FC model), and pH changes were recorded using a pH meter. To enhance the homogeneity of the solution, magnets were placed inside the anode and cathode chambers, and the entire EDM cell was mounted on a magnetic stirrer.

2.3. Setup

The EDM cell used in this study was constructed from Plexiglas and consisted of four distinct chambers: an anode chamber (75 mL capacity), a cathode chamber (75 mL capacity), and a dual-function production/desalination chamber (37 mL capacity). A graphite electrode (3 × 2 cm) was installed in the anode chamber, while the cathode chamber contained a titanium electrode (3 × 3 cm). An external power supply (MP-3005D) was connected to generate the required electric potential difference across the system. The cell configuration consisted of two cation-exchange membranes and one anion-exchange membrane, enabling efficient ion separation and PG production. Experimental trials were conducted using three distinct initial feed concentration settings (IFCSs) in the anode, cathode, and desalination chambers: IFCM1 (0.1 M, 0.1 M, 0.1 M), IFCM2 (0.5 M, 0.5 M, 0.1 M), and IFCM3 (0.1 M, 0.1 M, 0.5 M) respectively. The applied voltages of 5 V and 10 V were tested, and DI water was used in the product chamber to ensure purity and minimize contamination. A schematic representation of the experimental setup is provided in Fig. 1, which offers a clear and comprehensive visualization of the EDM configuration, flow pathways, and overall operational design.

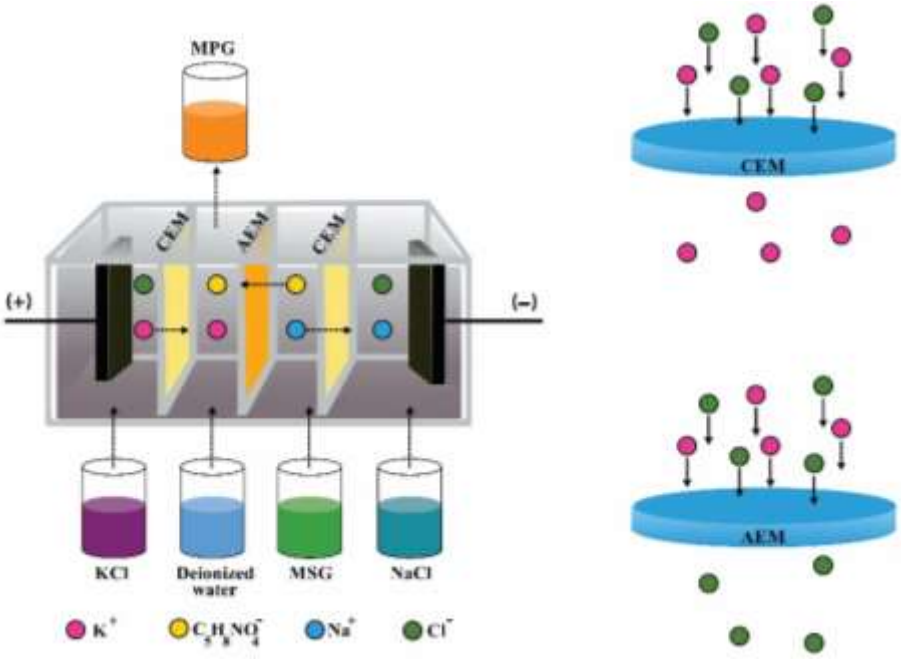

Figure 1. Schematic of the EDM process used in this study.

2.4. Preparation of the anion and cation exchange membranes

PVC-based IEMs containing MWCNT loadings of 0 wt% (M1), 4 wt% (M2), 8 wt% (M3), and 10 wt% (M4) were fabricated via the solution casting method. Initially, PVC was dissolved in THF under continuous magnetic stirring for 1 h at room temperature to obtain a homogeneous polymer solution. After complete dissolution, the anion and cation

exchange resins were gradually introduced into the solution and the mixture was stirred for an additional 2 h to ensure uniform dispersion within the polymer matrix. Subsequently, predetermined amounts of MWCNTs were added and the suspension was further stirred for 1 h. To enhance nanotube dispersion and reduce agglomeration, the mixture was subjected to ultrasonication for 75 min, followed by an additional stirring step to maintain homogeneity prior to casting. All preparation steps were carried out at ambient temperature.

The resulting homogeneous solution was cast onto clean glass plates using a casting applicator to achieve a uniform thickness of approximately 100 μm. The solvent was then allowed to evaporate slowly at room temperature to form stable membrane films. The cast membranes were subsequently immersed in a DI water coagulation bath at ambient temperature to induce phase inversion. The membranes were then rinsed, cut into the required dimensions, and stored in DI water for further characterization and performance evaluation [7,15]. Fig. 2 illustrates the IEM fabrication process.

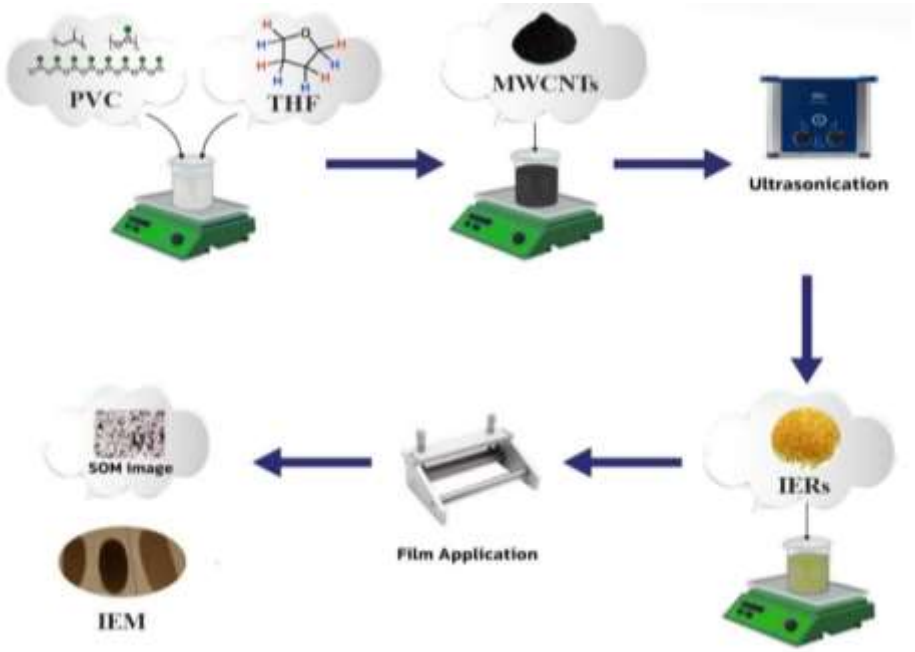

Figure 2. Membrane manufacturing steps.

2.5. Analysis and calculation

2.5.1. Membrane characterization

2.5.1.1. Hydrophilicity/Hydrophobicity

The interaction performance of a membrane with solvents and solutes is largely governed by its surface wettability, which is defined by its hydrophilicity/hydrophobicity nature. The degree of the hydrophilicity or hydrophobicity of the membrane surface was assessed by measuring the contact angle (θ). Contact angle measurements were performed at room temperature using the static water droplet method on dry IEMs samples. The behavior of a water droplet on the surface of IEMs provides both the qualitative and quantitative indications of their wettability characteristics [14].

2.5.1.2. Water Sorption

The water sorption capacity of the IEMs was evaluated by calculating the ratio of the absorbed water mass (in mg) to the dry mass

of the membrane samples, as defined in Eq. 1. This was determined based on the weight measurements conducted before and after drying. Prior to testing, all IEM samples were immersed in DI water for 48 hours to ensure complete hydration. After immersion, the surface moisture was gently removed using tissue papers, and the samples were immediately weighed. The membranes were then dried in an oven at 70 °C until a constant weight was achieved. The interaction behavior of the IEMs with solvents and solutes is significantly influenced by their hydrophobicity/hydrophilicity nature, which is characterized by the contact angle (θ) measurement [14].

$$WS = \frac{W_{wet} - W_{dry}}{W_{dry}} \times 100 \quad (1)$$

2.5.1.3. Area-Specific Resistance (ASR)

Measuring the ASR of IEMs is a key parameter for assessing the energy consumption of EDM systems. ASR measurements were conducted using a 0.5 M NaCl solution and an alternating current (AC) bridge. The total system resistance (R_1) was measured with the membrane placed inside the electrochemical cell containing the electrolyte solution. Subsequently, the cell resistance without the membrane (R_2) was measured under identical conditions. The membrane's intrinsic electrical resistance was then calculated using the following equation [34]:

$$R_m = (R_1 - R_2) \quad (2)$$

R_m can be used to measure the areal resistance (r) as:

$$\text{r } (\Omega.cm^2) = (R_m.\text{A}) \quad (3)$$

where A is the effective membrane area (in cm^2).

2.5.1.4. Tensile Strength

The tensile strength of the IEMs was assessed by cutting the samples to specified dimensions and evaluating their tear resistance at room temperature [14]. For the dry hollow fiber IEMs, tensile properties were measured at room temperature using a Shimadzu Universal Testing Machine EZ-LX (Kyoto, Japan) with a maximum load capacity of 5 kN, following the previously established procedure [5]. Membrane specimens with the dimensions of 30 × 20 mm were subjected to tensile testing to determine their tensile strength at the point of failure.

2.5.1.5. Structural and Morphological Characterization (FTIR and SEM)

The chemical structure of the prepared membranes was examined using the Fourier transform infrared spectroscopy (FTIR). The FTIR analysis was employed to identify the characteristic functional groups of the polymer matrix and to evaluate possible chemical interactions between the polymer chains and MWCNT nanoparticles.

The surface morphology and internal structure of the membranes were investigated using the scanning electron microscopy (SEM). The SEM analysis was used to evaluate the dispersion and distribution of MWCNTs within the polymer matrix and to examine the overall membrane morphology.

2.5.2 Chamber Product Analysis

The product compartment and desalination chamber of the EDM cell were investigated. Table 1 summarizes the parameters used to evaluate the performance of both the production and desalination chambers [35].

Table 1.
Expressions used to evaluate the electrodialysis EMD cell performance

Name	Formula	Parameters
Yield (%)	$R_t\% = \frac{C_t V_{pt}}{C_0 V_{f0}} \times 100$	C_t= Molar concentration of potassium ions at time t in the product chamber (g. L^{-1}). C_0=Initial molar concentration of glutamate ions in the feed chamber (g. L^{-1}). V_{pt}= The volume of the product chamber (L). V_{f0}= The volume of the feed chamber (L).
Energy consumption, (kWh.kg^{-1})	$E = \int_0^t \frac{UIdt}{C_t V_{pt}}$	U= applied voltage (V). I= electrical current (A)
Current efficiency (%)	$CE\% = \frac{ZFV_{pt}C_t}{NM \int I(t)dt} \times 100$	Z= Ionic charge. F= Faraday's constant (26.8 A. h. mol^{-1}). N= The number of IEM pairs. M= PG molecular weight (185.22g. mol $^{-1}$).
Salt removal efficiency (SRE,%)	$\%R_i = \left(1 - \frac{C_t}{C_0}\right) \times 100$	C_t= Salt concentration at time t in the feed chamber ($g.L^{-1}$). C_0= Initial salt concentration in the feed chamber ($g.L^{-1}$).
Salt removal rate (SRR, $\boldsymbol{g.m^{-2}.h^{-1}}$)	$SRR = \frac{(C_0 - C_t)V}{\Delta t.S}$	Δt= Experimental time (h). S= Membrane area (m^2). V_f= The volume of desalination chamber (L).

3. Result and Discussion

MWCNTs were employed in the fabrication of membranes with various compositions. The primary aim of this study was to investigate the influence of voltage fluctuations on the product efficiency and yield during the desalination process, in three different initial concentrations specific to each compartment (CSICs) for the anode, cathode, and desalination chambers: (CSIC1) 0.1, 0.1, 0.1 M; (CSIC2) 0.5, 0.5, 0.1 M; and (CSIC3) 0.1, 0.1, 0.5 M. Additionally, the effect of the operation time on product yield was examined. The key parameters monitored included the applied voltage, pH levels in the anode and cathode chambers, current generation, and TDS in both the desalination and production chambers. Measurements were recorded at predetermined time intervals.

The results indicated that increasing the applied voltage resulted in a corresponding increase in current generation, in agreement with findings reported in the literature [35]. As expected, the pH in the anode compartment decreased due to the accumulation of hydrogen ions, while the cathode compartment exhibited an increase in pH due to the production of hydroxide ions [14,36]. Furthermore, voltage levels were positively correlated with current output, as illustrated in Fig. 3 and Fig. 4 [37].

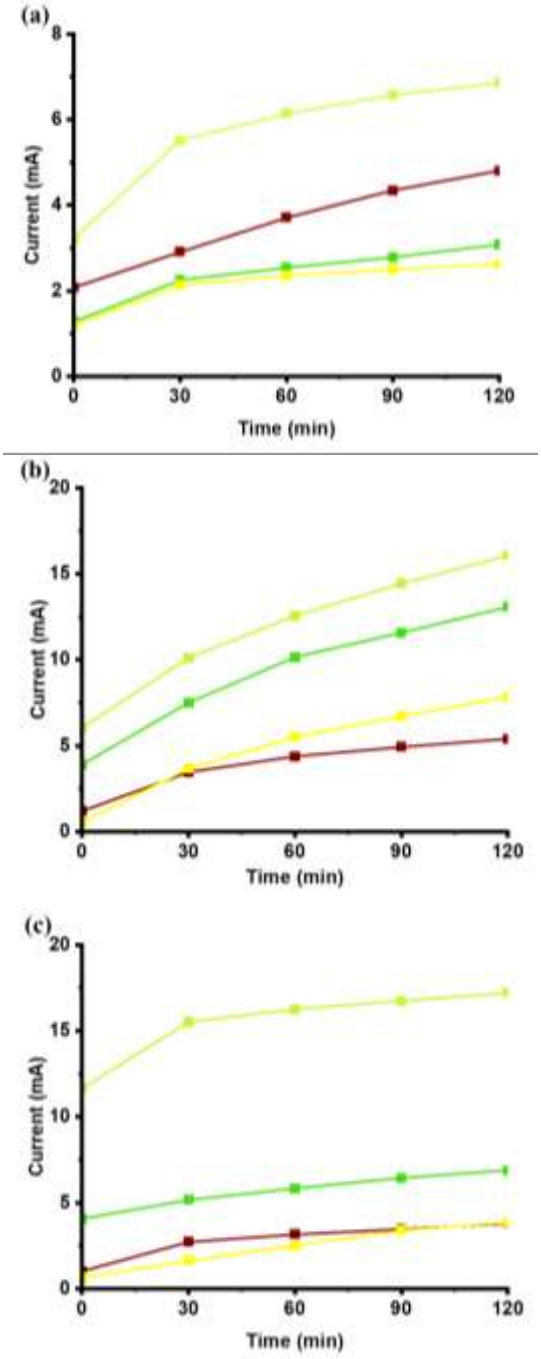

Figure 3. Effect of the type of CSICs (a: CSIC1, b: CSIC2, and c: CSIC3) and IEMs (M1: —■—, M2: —■—, M3: —■—, and M4—■— :) on the electric current under an applied voltage of 5V.

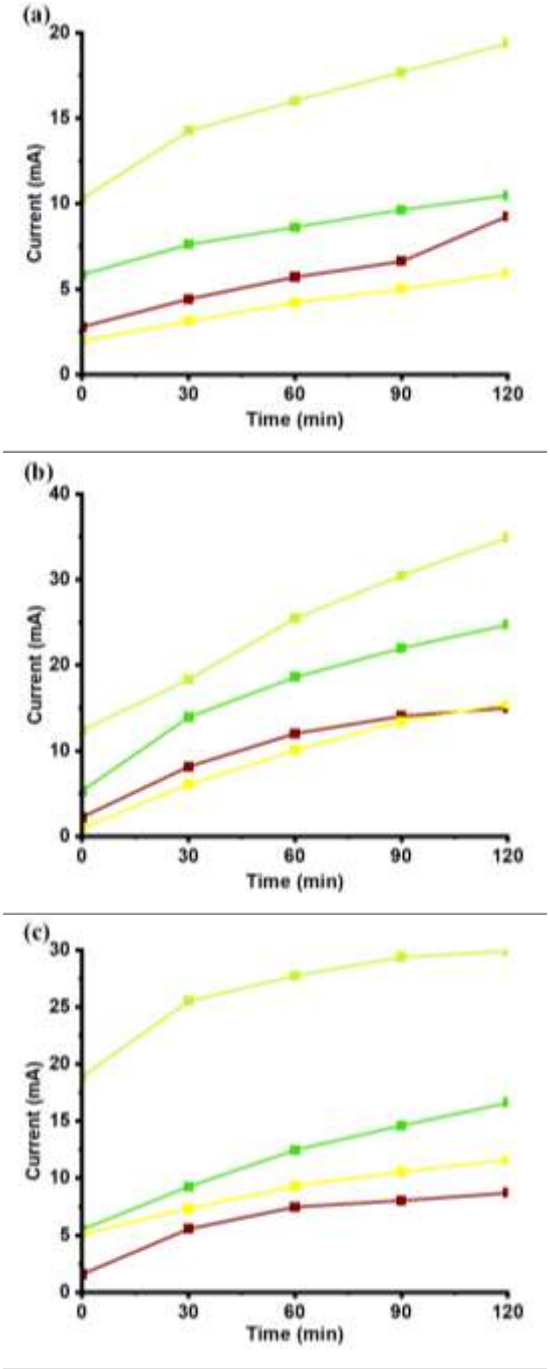

Figure 4. Effect of the type of CSICs (a: CSIC1, b: CSIC2, and c: CSIC3) and IEMs (M1: —■—, M2: —■—, M3: —■—, and M4: —■—) on the electric current under an applied voltage of 10V.

3.1. Membrane analysis

3.1.2. Hydrophilicity/Hydrophobicity

Table 2 shows that the contact angle of both AEMs and CEMs increases progressively with the higher content of MNCNTs. This trend confirms that the incorporation of MNCNTs into the solution alters the surface free energy of the IEMs, imparting greater hydrophobicity. The gradual rise in the contact angle suggests that MWCNTs are reasonably well-dispersed within the polymer matrix, contributing both to chemical modification of the surface and to an increase in nanoscale roughness. Such modifications are expected to influence key

membrane properties: reduced surface wettability may suppress excessive water sorption and swelling, while simultaneously affecting ionic transport pathways. Therefore, while the hydrophobic reinforcement caused by MNCNTs may enhance dimensional stability and potentially improve resistance to fouling, an optimal MWCNT loading must be identified to balance surface hydrophobicity with ion-exchange performance [38].

Table 2.
Results of the contact angle measurements for the fabricated AEMs and CEMs

Contact angel				
Membrane	**M1**	**M2**	**M3**	**M4**
Anionic	50	60	63	70
Cationic	40	57	65	70

3.1.1. Water sorption

Figs. 5a and 6a show the water sorption of the fabricated AEMs and CEMs, indicating a decrease in water sorption by increasing the content of MWCNTs. For the AEMs, water sorption decreases sharply from approximately 220% in the pristine sample (M1) to about 50% in the membrane containing 8 wt% MWCNTs (M3), followed by a slight increase at 10 wt% (M4). CEMs exhibit a similar trend, though with lower overall water sorption values (maximum ~100% for M1 and minimum ~40% for M3). This reduction is attributed to the enhanced polymer network density, decreased membrane matrix polarity due to strong MWCNT-polymer interactions, and tortuous diffusion pathways created by well-dispersed MWCNTs. The slight increase at 10 wt% MWCNT loading (M4) likely results from nanotube agglomeration, creating microstructural heterogeneities that facilitate limited water sorption. These results align with the enhanced hydrophobic character of the membranes upon the incorporation of MWCNT into the solution. The nonpolar nature of nanotubes reduces polar sites for hydrogen bonding, confirming increased hydrophobicity and compactness. Overall, adding MWCNTs effectively enhances the structural integrity and hydrophobicity of the fabricated IEMs. The observed difference between AEMs and CEMs suggests that the nature of the ionic functional groups significantly influences water sorption, with AEMs exhibiting a higher affinity for water. These findings confirm that adding MWCNT is a promising approach for tailoring the hydrophilic/hydrophobic balance and improving the dimensional stability of the IEMs. [39].

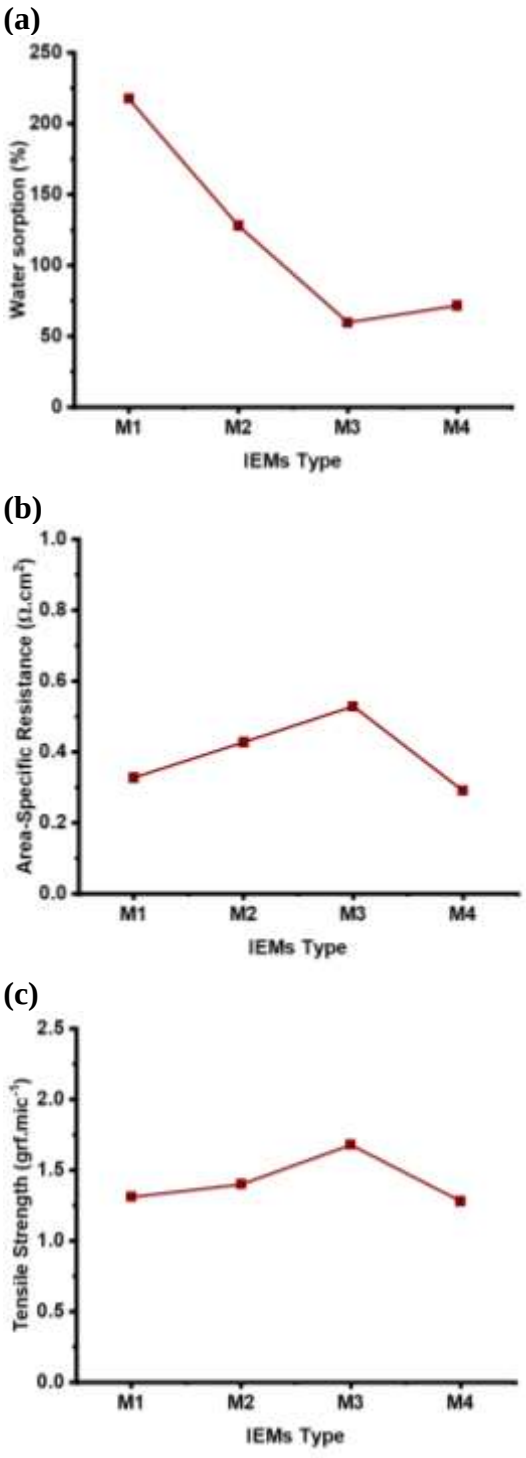

Figure 5. Measured properties of the fabricated AEMs based on PVC/MWCNTs composites: (a) water sorption, (b) area resistance, and (c) mechanical resistance.

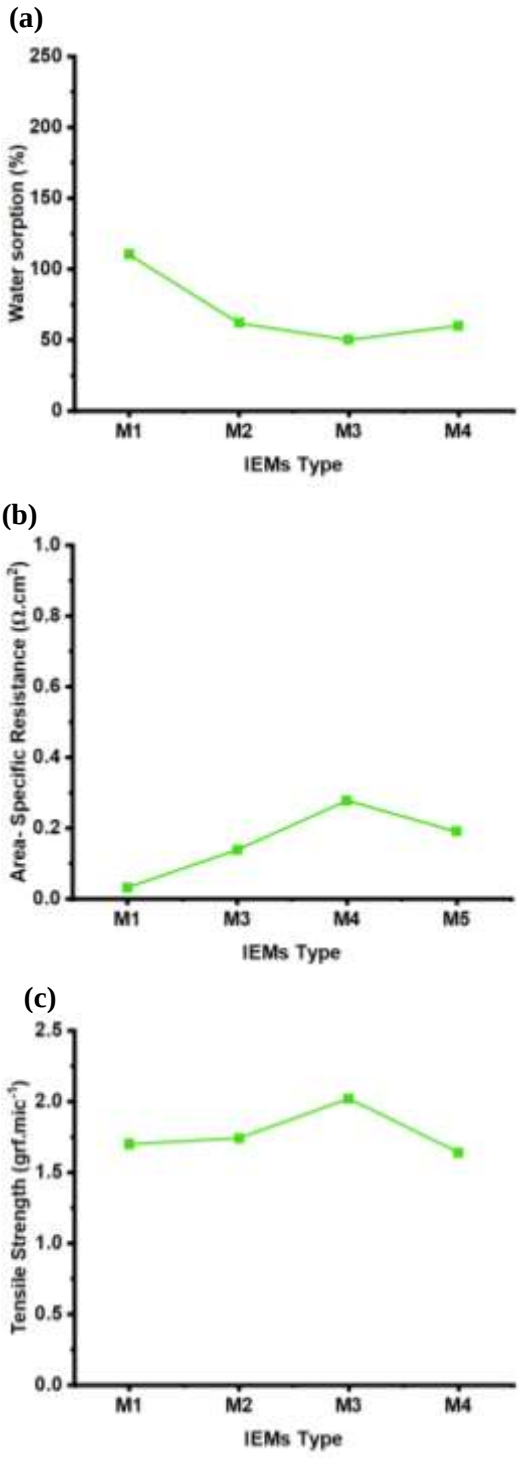

Figure 6. Measured properties of the fabricated CEMs based on PVC/MWCNTs composites: (a) water sorption, (b) area resistance, and (c) mechanical resistance.

3.1.3. Area-Specific Resistance (ASR)

Figs. 5b and 6b show the area-specific resistance (ASR) of the fabricated AEMs and CEMs. Both membrane types exhibit a non-linear ASR trend by increasing the content of MWCNT. For AEMs, ASR increases from the pristine membrane (M1) to 8 wt% MWCNTs (M3) and then decreases at 10 wt% (M4).

CEMs show a similar trend, with ASR rising from M1 to M4 before slightly declining. The initial increase in ASR is attributed to the reduced water content and increased polymer network compactness due to the enhanced hydrophobicity caused by the addition of MWCNT, limiting water sorption and hydrated ionic pathways. The subsequent decrease in ASR at higher loadings (>8 wt%) of MWCNTs likely results from the formation of conductive percolation pathways, facilitating charge transfer and improving conductivity. Furthermore, excessive amounts of MWCNTs can cause agglomeration, creating microvoids that enhance local ion mobility, reducing resistance. These results demonstrate that adding MWCNT significantly affects the electrochemical properties of the fabricated IEMs. The optimal amount of MWCNT balances increased compactness and hydrophobicity (increased ASR) with the formation of conductive pathways at higher loadings (lowering ASR). The slight differences between AEMs and CEMs suggest that the type of ionic functional groups and their interaction with MWCNTs influence ion transport resistance [14,39,40].

3.1.4. Tensile Strength

Figs. 5c and 6c compares the tensile strength of the fabricated IEMs. The results of tensile strength measurements (grf·mic^{-1}) reveal that adding MWCNTs has significant effects on the mechanical properties of IEMs. In the pristine sample (M1), the tensile strength of CEMs is higher than that of AEMs (≈1.7 vs. 1.3 grf·mic^{-1}). By adding MWCNTs (M2 and M3), both membranes exhibit an upward trend in tensile strength. At this stage, MWCNTs act as reinforcing agents, causing a remarkable enhancement in mechanical properties. The maximum tensile strength for both IEMs is observed in M3 (≈2.0 grf·mic^{-1} for the CEM and ≈1.65 grf·mic^{-1} for the AEM). These results confirm the reinforcing effect of MWCNTs in improving the polymer structure and enhancing mechanical resistance. Finally, at higher loading of MWCNTs (10%, M4), the tensile strength of both CEM and AEM decreases, returning to the values close to those of the pristine IEMs. This deterioration can be attributed to the aggregation of MWCNTs at high concentrations, which introduces weak zones within the polymer matrix and reduces structural integrity.

Overall, the findings demonstrate that the addition of MWCNTs up to an optimal concentration (≈8%) strengthens the tensile properties of IEMs. However, the excessive loading leads to the agglomeration of MWCNTs and reduced structural uniformity, resulting in a decline in mechanical strength. Furthermore, at all stages, CEMs consistently exhibit higher tensile strength compared to AEMs, indicating the superior compatibility of the cationic polymer matrix with MWCNTs [14].

3.1.5. FTIR and SEM analysis

The FTIR spectra of the neat PVC membrane (Fig. 7a) and the PVC/MWCNT (8 wt%) membrane (Fig. 7b) were analyzed to evaluate structural changes and intermolecular interactions within the polymer matrix. In both spectra, a broad absorption band in the range of 3300-3260 cm^{-1} is attributed to O–H stretching vibrations, arising from the absorbed moisture, hydroxyl groups of the cationic resin, and hydrogen-bonding interactions. A slight shift toward lower wavenumbers in the MWCNT-containing membrane suggests the enhanced intermolecular interactions between carbon nanotubes and PVC chains.

The bands observed at 3020-2910 cm^{-1} correspond to the aliphatic and vinyl C–H stretching vibrations of the PVC backbone and residual THF solvent. Minor shifts and

intensity variations after adding MWCNT indicate changes in the local chemical environment and reduced polymer chain mobility. The peak at approximately 1614-1612 cm^{-1} is assigned to C=C skeletal vibrations, with increased intensity in the modified membrane confirming the presence of graphitic carbon structures caused by MWCNTs. The region between 1476 cm^{-1} and 1426 cm^{-1} is associated with CH_2 bending and PVC chain vibrations, where slight shifts further indicate the physical interactions between MWCNTs and the polymer matrix. Bands in the 1328-1248 cm^{-1} and 1100-1000 cm^{-1} regions correspond to C–O and C–C stretching vibrations, likely related to the resin phase and residual solvent effects, with intensity changes reflecting the modifications in polymer chain arrangement and improved structural compactness.

Finally, peaks in the 900-700 cm^{-1} range are attributed to C–H out-of-plane bending and C–Cl stretching vibrations characteristic of PVC. The slight sharpening and shifting of these bands after the addition of MWCNT suggest restricted chain mobility and increased structural ordering. Overall, the FTIR results confirm that no new chemical bond was formed, indicating that MWCNTs were added primarily through physical interactions and van der Waals forces, while significantly influencing the membrane microstructure.

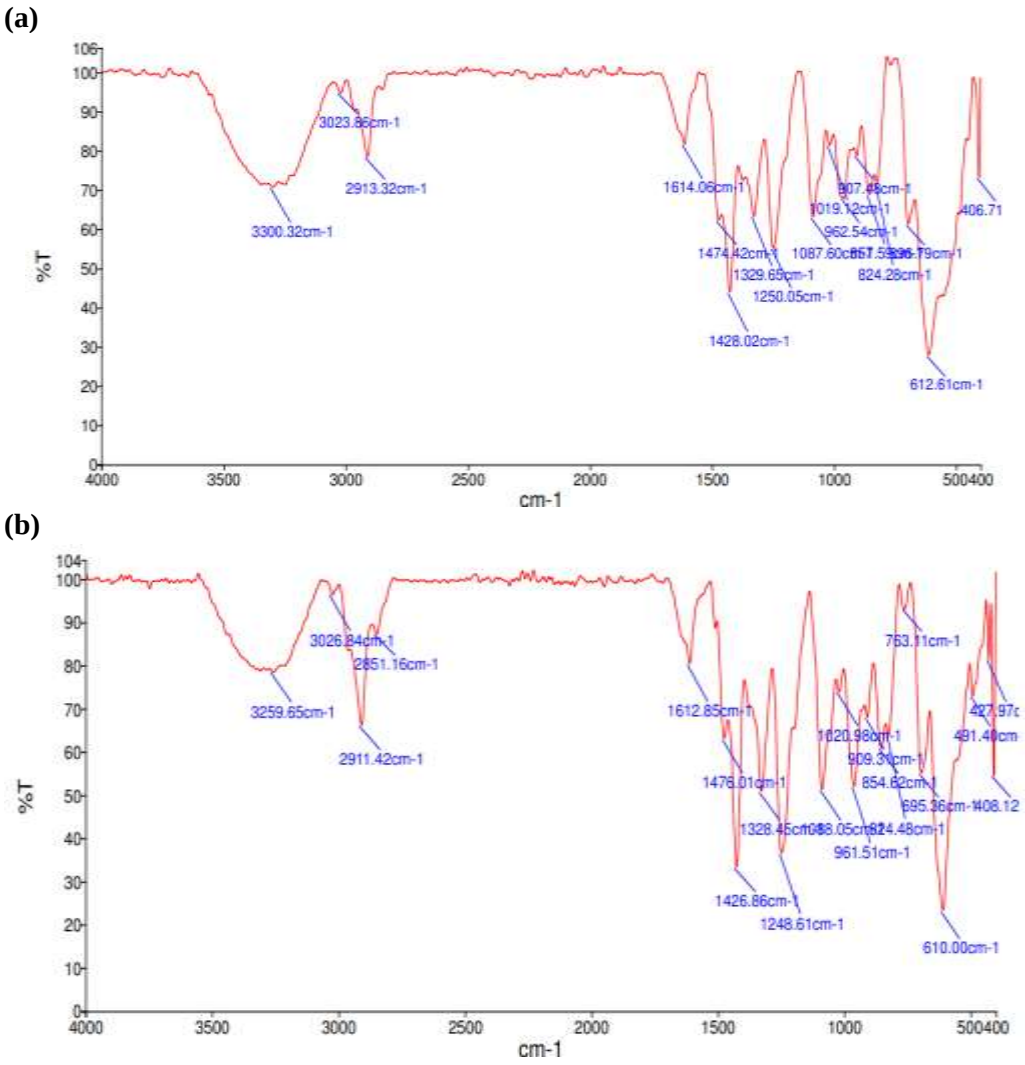

Figure 7. FTIR spectra of the prepared membranes: (a) PVC membrane without MWCNTs and (b) PVC/MWCNT (8 wt%) nanocomposite membrane.

The SEM images of the pristine PVC membrane (Fig. 8a) and the PVC/MWCNT membrane containing 8 wt% MWCNT (Fig. 8b) were analyzed at magnifications of 25x, 30x, and 100x to evaluate the effect of the addition of MWCNT on the morphology of membranes. The pristine PVC membrane exhibits a relatively rough and heterogeneous surface with irregular domains and localized protrusions. At higher magnification, surface defects and non-uniform regions become more evident, which can be attributed to solvent evaporation during the phase inversion process and the intrinsic morphology of PVC-based membranes.

In contrast, the PVC/MWCNT membrane shows a more compact and homogeneous surface morphology across all magnifications. The addition of MWCNTs reduces surface irregularities and results in a finer and more uniform texture. At 100x magnification, the modified membrane appears denser and smoother compared to the pristine membrane, indicating improved structural organization. This morphological improvement is attributed to the effective interaction between MWCNTs and PVC chains, which enhances matrix integrity and suppresses defect formation during membrane casting. The absence of the noticeable agglomeration of MWCNTs further confirms the good dispersion of MWCNTs within the polymer matrix.

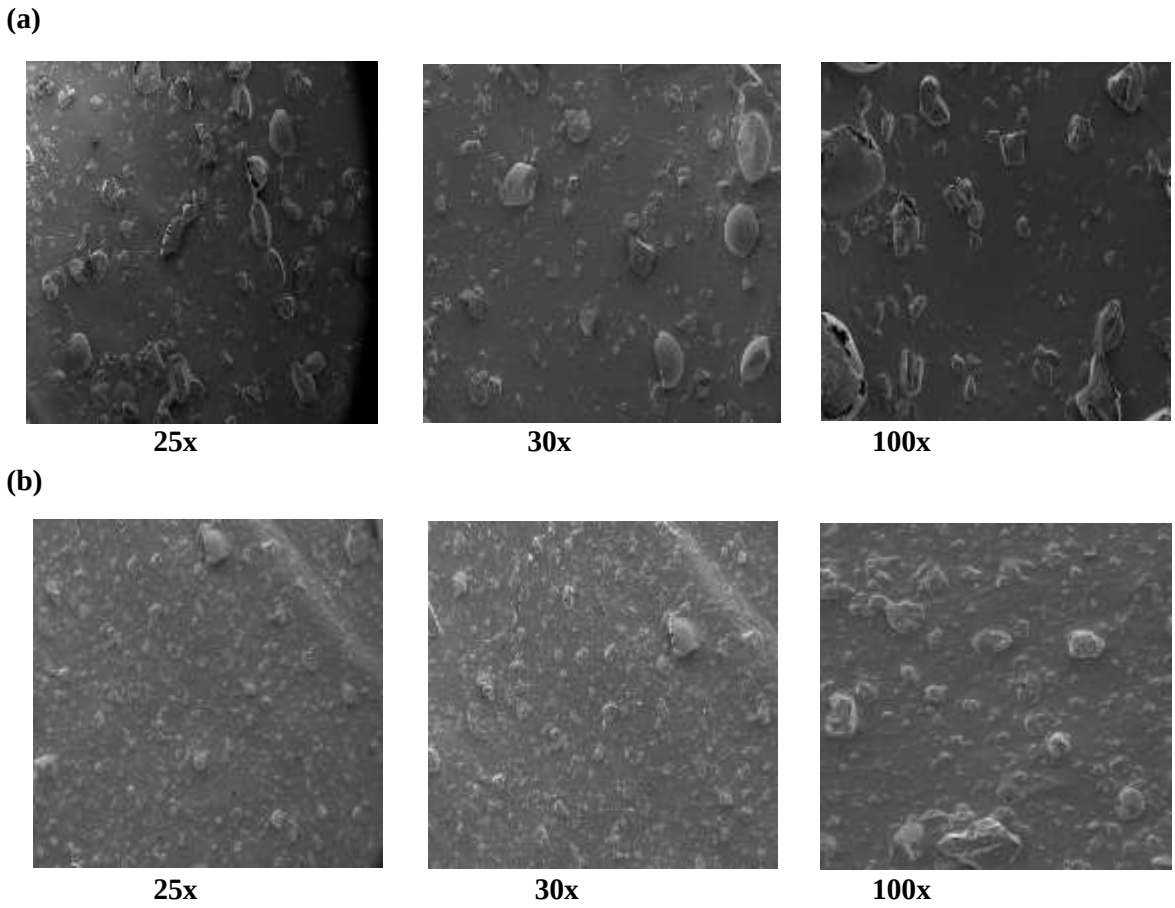

Figure 8. SEM micrographs of the prepared membranes at different magnifications (25×, 30×, and 100×): (a) PVC membrane without MWCNTs and (b) PVC/MWCNT (8 wt%) nanocomposite membrane.

3.1.6. Comparative Performance of the Prepared PVC/MWCNT IEMs

Compared with the commercial and reported synthetic IEMs, as presented in Table 3, the PVC/MWCNT IEMs prepared in this work exhibit distinctive performance characteristics. The water contact angle increased from 40° to 70° by increasing the amount of MWCNT, indicating tunable surface wettability, in contrast to the same in some reported membranes such as PES/PANI-co-MWCNT (46.8-63.4°). The water uptake (50-200%) was significantly higher than that of PES/PANI-co-MWCNT (72-73%) and PPO/sCNT (42.3-53.8%), suggesting enhanced hydration capability. The electrical resistance of the fabricated membranes (0.05–0.6 Ω·cm²) was considerably lower than those of Nafion 117 (1.8-3.2 Ω·cm²), Nafion 115 (1.5-2.2 Ω·cm²), CMX (2.2-2.6 Ω·cm²), PPA/MWCNT (13-25 Ω·cm²), and PVC/AC-co-CS (13-21 Ω·cm²), indicating favorable ion transport and reduced ohmic losses. Overall, PVC/MWCNT IEMs demonstrate a favorable combination of high water uptake, low electrical resistance, adequate mechanical stability, and tunable wettability, making them promising candidates for advanced ion separation and electro-membrane applications.

Table 3.
Comparison of some characteristics of commercial and synthetic membranes

Membrane	Water uptake (%)	Electrical resistance $(\Omega.cm^2)$	Contact angle (°)	Ref.
Nafion 117	11.7	1.8-3.2	–	[48]
CMX	25.5	2.2-2.6	–	[48]
Nafion 115	11.2	1.5-2.2	–	[48]
Fuji-CEM	34	2.4-9	–	[48]
PVC/AC-co-CS	12-21	13-21	62-80	[49]
PPO/sCNT	42.3-53.8	1-19-1.39	–	[50]
PVDF/NWCNTs/SiO_2	–	–	84-92	[51]
PPA/MWCNT	13-17	13-25	–	[52]
PES/PANI-co-MWCNT	72-73	–	46.76-63.43	[53]
PVC/MWCNT	50-225	0.05-0.06	40-70	This work

3.2. Production analysis

A systematic experimental investigation was carried out to evaluate the performance of electrodialysis (ED) cells in the synthesis of target products. The study initially focused on concentration changes over a 2-hour period under varying conditions of feed concentration, membrane type, and applied voltage. Fig. 9 presents the results for the production of PG using different IEMs under the applied voltages of 5 V and 10 V, across three CSICs in the anode, desalination, and cathode chambers. According to the results, M3 was identified as the most effective, exhibiting the highest current response and the greatest concentration of PG in the production compartment. The results indicate that product yield increased by increasing voltage in the CSIC2 configuration. In contrast, under CSIC1 and CSIC3 conditions, an increase in voltage led to a reduction in the production rate of PG.

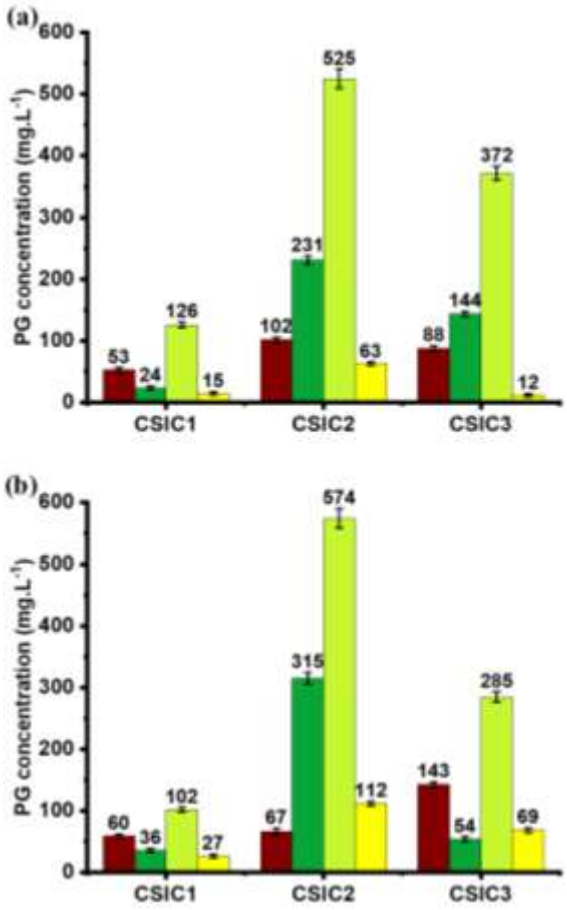

Figure 9. Concentration of PG in the production chamber after 2 h at the applied voltages of (a): 5 V and (b): 10 V under different CSICs. (M1: , M2: , M3: , and M4:).

Following the selection of the optimal IEMs (8% nanoparticle content, M3) for the enhanced production of PG, the production performance of PG was further evaluated at the applied voltages of 5 V and 10 V over a 4-hour period. The concentrations of potassium ions in the production chamber were quantified using a flame photometer, and key performance metrics, including product yield, current efficiency, and energy consumption, were systematically assessed.

The results of this study clearly demonstrate the significant influence of operating conditions, particularly the concentration of reactant solutions and the applied voltage, on the overall performance of the electrodialysis process for the production of potassium glutamate using IEMs. The comparison of the three experimental configurations (CSIC1, CSIC2, and CSIC3) provides valuable insights into the optimization of this process. As observed in the results, the CSIC2 condition, with higher concentrations of the electrolyte (0.5 M in both anode and cathode compartments) and an applied voltage of 10 V, achieved the highest production efficiency of PG (35.55%). This finding indicates that increasing both the electrochemical driving force and the availability of reactive ions plays a critical role in enhancing the efficiency of ion transport and conversion. Although the energy consumption under these conditions increased to 24.52 units, this rise appears justifiable when weighed against the substantially higher yield, representing an optimal balance between the energy input and product efficiency.

In contrast, the CSIC1 condition (0.1 M in all compartments and 5 V) resulted in relatively low efficiency (8.44%), despite lower energy consumption (11.73 units). This outcome highlights that at lower concentrations and voltages, mass-transfer limitations and insufficient driving force prevent the achievement of high yields. A further notable observation is the diminished performance observed under CSIC3 conditions (0.5 M in the desalination compartment, combined with lower concentrations of the electrolyte and 5 V), which yielded the lowest efficiency (3.83%). This result underscores the complexity of maintaining concentration balance across compartments and its effect on membrane-related phenomena and ion transport efficiency. It appears that increasing the concentration of target species in the desalination compartment, without proportionally raising the driving potential and electrolyte concentrations, may lead to membrane surface saturation or increased

resistance, ultimately reducing the overall process efficiency [41,42].

From an industrial perspective, the observed energy consumption values should be interpreted in the context of laboratory-scale operations, where energy requirements are typically higher due to limitations in cell geometry, membrane surface area, hydrodynamic conditions, and non-optimized operating parameters. In industrial electrodialysis and electro-membrane systems, the optimization of flow dynamics, membrane configuration, and current efficiency generally leads to a significant reduction in the specific energy consumption. Therefore, although the CSIC2 configuration exhibited higher energy consumption, its substantially improved PG production efficiency results in a more favorable overall energy-to-product ratio and demonstrates the potential applicability of the process for further scale-up and optimization. Figs. 10 and 11 summarize the performance outcomes in the production chamber.

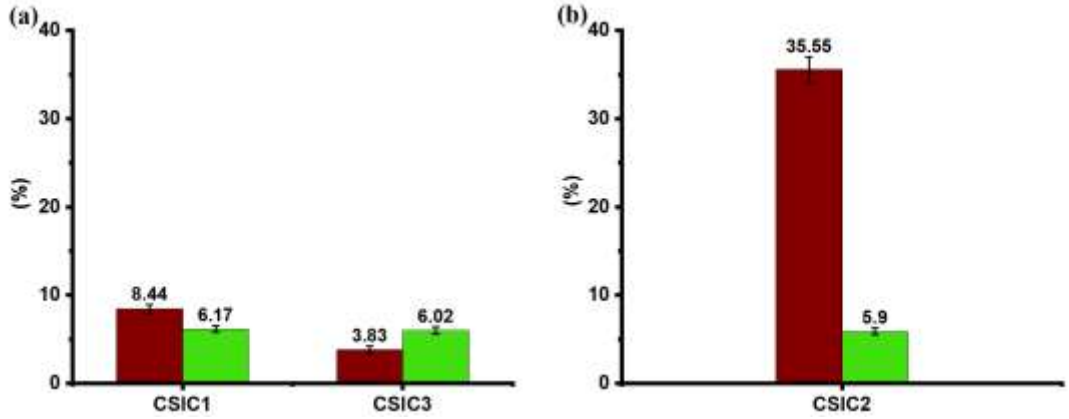

Figure 10. Yield ( ) and Current efficiency ( )for the production of PG in a: 5 V for CSIC1 and CSIC3, and b: 10V for CSIC2 with 8% membrane.

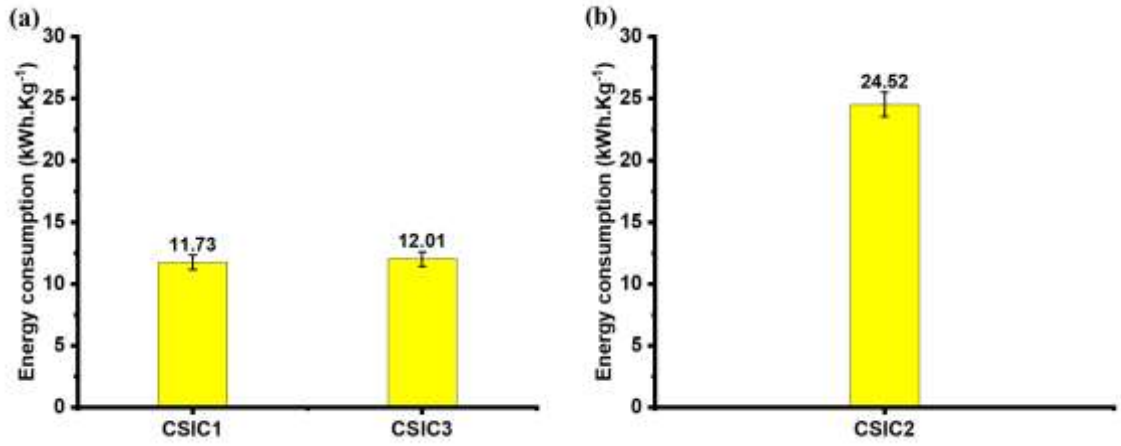

Figure 11. Energy consumption ( ) for the production of PG in a: 5 V for CSIC1 and CSIC3, and b: 10V for CSIC2 with 8% membrane.

3.3. Desalination analysis

3.3.1 Salt removal efficiency (SRE)

Fig. 12 illustrates the influence of the concentration of the feed, membrane type, and applied voltage on SRE. The key findings of this study highlight the significant impact of concentration configuration on process efficiency. At both applied voltages examined

(5 and 10 V), the CSIC1 configuration, characterized by low concentrations (0.1 M) in the anode, cathode, and desalination compartments, achieved the highest desalination efficiency (approximately 68% at 5 V and 66% at 10 V) utilizing M3. This observation indicates that under more dilute conditions, the transport of the target ions across IEMs toward the electrodes occurs more readily, likely due to a more favorable concentration gradient and lower resistance throughout the process. In contrast, increasing the concentrations of the electrolyte in the anode and cathode compartments to 0.5 M (CSIC2), as well as raising the concentration of sodium glutamate (SG) to 0.5 M (CSIC3), led to a substantial reduction in the desalination efficiency at both voltage levels. For example, at 5 V, the desalination efficiency decreased from 68% in CSIC1 to approximately 48% in CSIC2 and 47% in CSIC3. This performance decline can be attributed to several factors, including the ionic competition, increased electrical resistance, and reduced permeability of the target molecule. At higher concentrations, the competition between salt ions for passage through IEMs increases, potentially decreasing membrane selectivity. Moreover, Increasing the concentration of the solution can lead to higher electrical resistance across the electrodialysis cell. This increased resistance either requires a higher voltage to maintain the same current or results in the reduced current at a fixed voltage, ultimately negatively affecting desalination efficiency. At higher concentrations of SG (CSIC3), the likelihood of larger glutamate molecules penetrating the membrane or blocking membrane pores increases, further reducing salt separation efficiency.

The effect of increasing the applied voltage from 5 to 10 V was also investigated. The results indicated that this change does not significantly improve desalination efficiency. Even in the CSIC1 configuration, the efficiency slightly decreased from 68% to 66%. This phenomenon may be related to the membrane behavior at higher voltages, where the accumulation of ions near the membrane surface increases local resistance and reduces the effectiveness of ion transport [14,42].

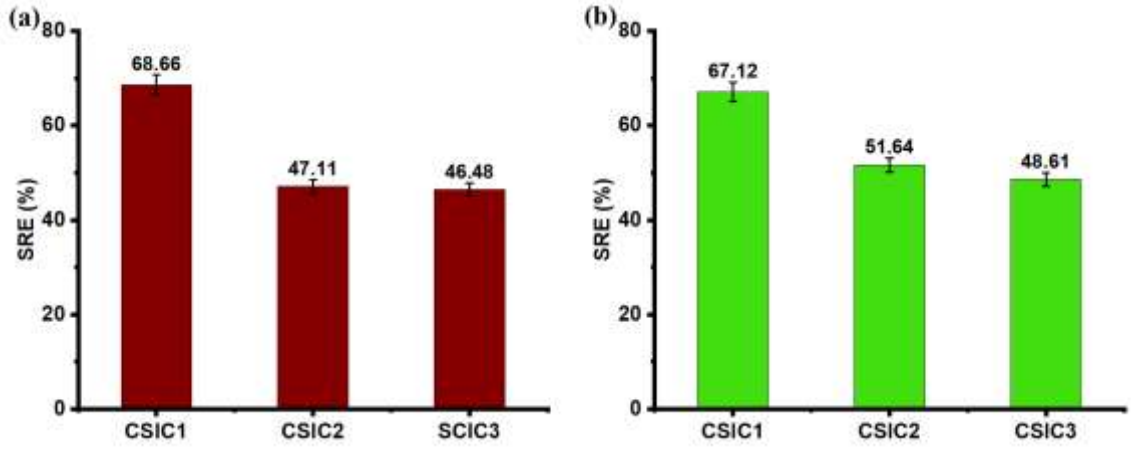

Figure 12. Effect of the applied voltage (a: 5 V, and b: 10 V) on the salt removal efficiency of the desalination chamber with various concentrations and 8% membrane.

3.3.2. Salt removal rate (SRR)

Fig. 13 depicts the SRR for M3 under different experimental conditions. Variations in SRR among these conditions are influenced by

multiple factors, such as the intrinsic characteristics of the membrane, the effect of voltage on ion transport mechanisms, fluctuations in output current with increasing voltage, the availability of electrolyte channels that enable the movement of ions, and the concentration gradients of the salt within the system [43,44].

SRR exhibited similar patterns at both the 5 V and 10 V applied voltages. The CSIC3 configuration, where the desalination chamber contained a higher concentration of the salt than the anode and cathode chambers, achieved the maximum SRR. This observation suggests that creating a concentration gradient between compartments provides an additional driving force, in addition to the electric field, for ion transport. In other words, the presence of a concentration gradient enhances the efficiency of ion transfer from the desalination compartment toward the anode and cathode compartments. This phenomenon was observed at both 5 V and 10 V, with the SRR slightly higher at 10 V. The increase in SRR at the higher voltage can be attributed to the stronger electric field, which facilitates the ionic movement. In contrast, the CSIC2 mode, with a relatively low concentration of the salt in the desalination chamber, resulted in the lowest SRR. However, the lower SSR of CSIC2 compared to that od CSIC1 can be attributed to the reduced mass transfer resistance under more dilute conditions, as well as to the minimization of disruptive effects such as the ionic accumulation near the membrane surface. Therefore, unlike the CSIC3 configuration, where the synergistic effect of the electric field and concentration gradient resulted in the highests SRR, increasing the voltage from 5 to 10 V in the CSIC1 and CSIC2 configurations did not produce a noticeable improvement in the salt removal performance. It should be noted that SRR reflects the instantaneous membrane performance and the initial ionic flux, whereas SRE represents the overall process performance and the total amount of ions transferred. The discrepancy between these two parameters arises from the effect of the concentration, local resistance, ionic accumulation, and limitations in membrane selectivity [43,44].

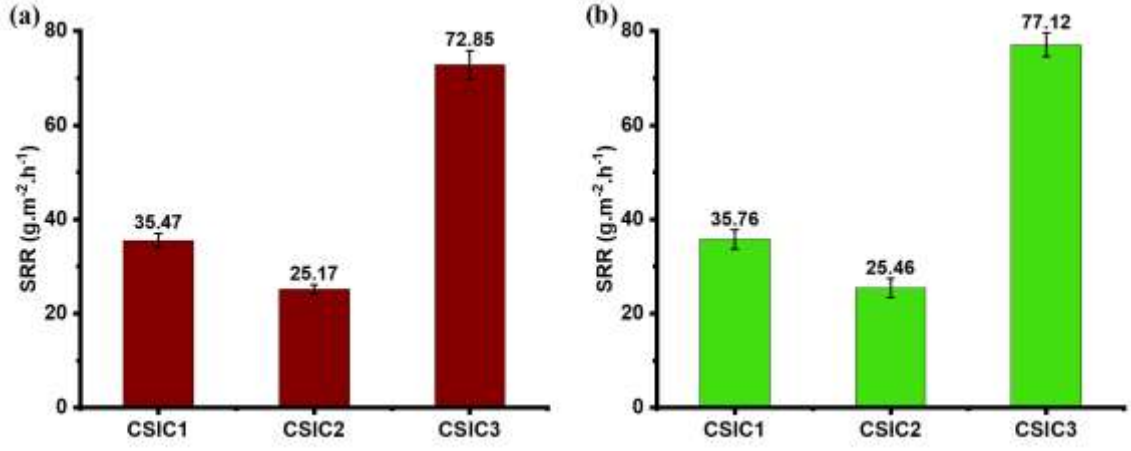

Figure 13. Effect of the applied voltage (a: 5 V, b: 10 V) on the salt removal rate for desalination chambers with various concentration.

3.4. Optimal voltage and anode/cathode concentrations

Building on the strong performance of M3, the influence of the applied voltage of 15 V on the

SRE in the desalination chamber and the changes in the concentration of PG in the product chamber were examined. These results were compared with those obtained at 5 and 10 V. As shown in Fig. 14, the experiments conducted for ISIC1 at 15 V demonstrated lower yield and product output than at lower voltage conditions (5 and 10 V).

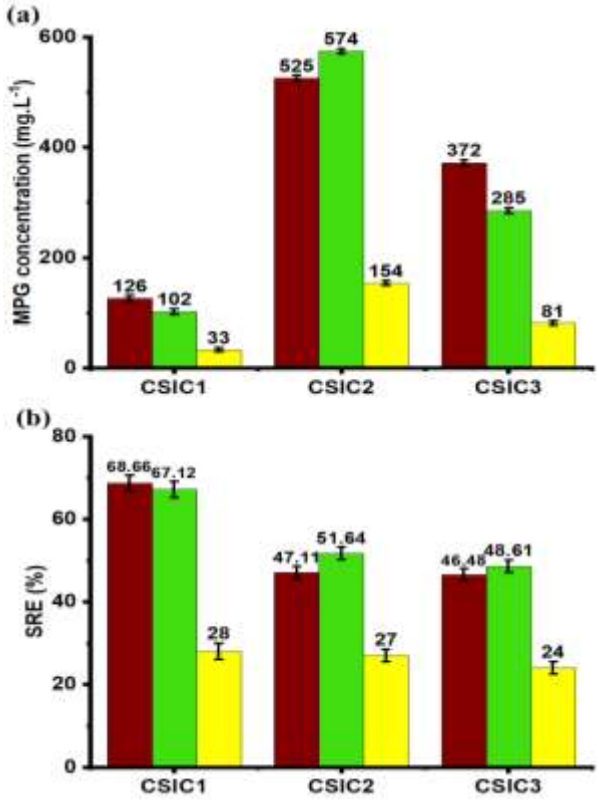

Figure 14. Comparison of a: PG concentration changes and b: SRE at different voltages (5V: ▬, 10V: ▬, and 15V: ▬) in the M3 membrane.

This reduction in the performance at higher voltages can be attributed to the concentration polarization and the accumulation of deposits on the IEMs surfaces, which collectively reduce the dehumidification rate and production efficiency. The elevated voltage accelerates the migration of ion ions toward IEMs, resulting in an increased accumulation of ions at the membrane surfaces. Consequently, this leads to a higher ionic concentration at the interfaces between IEMs, causing an increase in electrical resistance. The heightened resistance impedes ion transport across IEMs, thereby diminishing the overall process efficiency. Additionally, the deposition of ions on the IEMs surfaces at high voltages further obstructs the movement of ions and exacerbates the decline in efficiency [45]. In CISC2, raising the voltage from 5 to 10 V resulted in enhancing the production of PG and improving SRE. However, further increasing the voltage to 15 V caused a decline in both parameters. This reduction is likely due to the predominance of the adverse high-voltage effects, such as the increased leakage currents, ohmic heating, and decreased membrane selectivity. In the case of CSIC3, the increase in the voltage produced different effects. Increasing the voltage from 5 to 10 V led to a decrease in the production of PG, while for SRE, a slight improvement was observed. Nevertheless, further increasing the voltage to 15 V resulted in a significant drop in the desalination efficiency, indicating the operational limitations of the process at high voltages.

The results in Figs. 9, 10, and 11 show that the highest PG production occurred when high concentrations were applied in both the cathode and anode chambers relative to the desalination chamber (CSIC2), with the M3 AEM/CEM pair identified as optimal at 10 V. Therefore, a further comparative investigation was conducted to determine the optimal initial concentrations of the cathode and anode chambers, using 0.4 and 0.6 M solutions. According to the results shown in Table 4, the greatest increase in the concentration of PG was recorded at the concentration of 0.5 M, reaching 574 $mg \cdot L^{-1}$ (Fig. 9b). Furthermore, SRE was significantly enhanced when both anode and cathode concentrations were maintained at 0.5 M, achieving a desalination effect value of 51.6, which exceeded those observed under other tested conditions [46,47].

Table 4.
SRE% and the concentration of PG for the CSIC2 configuration with M3 IEMs: Effect of the concentrations of cathode and anode.

CSISs (mol.L^{-1})			SRE (%)	PG Concentration (mg.L^{-1})
Anode	Cathode	Desalination		
0.4	0.4	0.1	39	125
0.5	0.5	0.1	51.6	574
0.6	0.6	0.1	48.1	234

This finding indicates the presence of optimal concentrations in the anode and cathode compartments. At lower concentrations (0.4 M), the concentration gradient provides an insufficient driving force, resulting in mass transfer limitations. In contrast, at higher concentrations (0.6 M), effects such as the ionic aggregation, increased electrical resistance, and reduced membrane selectivity are likely to occur, causing a decline in performance. Thus, the intermediate concentration of 0.5 M offers a more favorable balance between the ionic driving force and system stability, ultimately yielding the highest production and desalination efficiency [47].

4. Conclusions

This study investigated the effectiveness of EDM for the simultaneous desalination and chemical synthesis using PVC/MWCNTs-based AEMs and CEMs. IEMs with varying loadings of MWCNTs were compared with pristine PVC IEM (M1), and the performance was evaluated under different concentrations of anode, desalination, and cathode chambers at 5 and 10 V. The M3 membrane containing 8% MWCNTs exhibited the highest production of PG, with maximum yields occurring when the of the anode and cathode exceeded that of the desalination compartment (CSIC2). M3 also consistently achieved the highest SRE across concentration ranges, while the optimal desalination was observed under lower concentration of the anode and cathode (CSIC3). The enhanced SRE was attributed to the increased hydrophobicity of the MWCNT-modified IEMs, as reflected by greater contact angles.

Building on the strong performance of M3, further investigation revealed that both the production of PG and SRE were highly dependent on the applied voltage and initial concentrations of compartments. The highest yield of PG and SRE (574 mg·L^{-1} and 51.6, respectively) were obtained at 10 V with an intermediate concentration of 0.5 M, whereas higher voltages (15 V) did not improve the performance. These results underscore the importance of optimizing both the voltage and concentrations of compartments to maximize the efficiency of simultaneous desalination and chemical production using the fabricated IEMs and CSIC configurations.

Acknowledgments

We sincerely thank and appreciate the University of Kashan for its partial financial support of this work.

Competing interests

The authors declare that they have no financial or non-financial competing interests.

Data Availability and Reproducibility

All data, experimental procedures, and analytical methods supporting the findings of this study are available from the corresponding author upon reasonable request.

Reference

[1]Liu L, Cheng Q. Mass transfer characteristic research on electrodialysis for desalination and regeneration of solution: A comprehensive review. Renew Sustain Energy Rev 2020;134:110115. https://doi.org/https://doi.org/10.1016/j.rser.2020.110115.

[2]Carstea EM, Bridgeman J, Baker A, Reynolds DM. Fluorescence spectroscopy for wastewater monitoring: a review. Water Res 2016;95:205–19. https://doi.org/https://doi.org/10.1016/j.watres.2016.03.021.

[3]Elgallal M, Fletcher L, Evans B. Assessment of potential risks associated with chemicals in wastewater used for irrigation in arid and semiarid zones: A review. Agric Water Manag 2016;177:419–31. https://doi.org/https://doi.org/10.1016/j.agwat.2016.08.027.

[4]Carolin CF, Kumar PS, Saravanan A, Joshiba GJ, Naushad M. Efficient techniques for the removal of toxic heavy metals from aquatic environment: A review. J Environ Chem Eng 2017;5:2782–99. https://doi.org/https://doi.org/10.1016/j.jece.2017.05.029.

[5]Tanaka Y. A computer simulation of continuous ion exchange membrane electrodialysis for desalination of saline water. Desalination 2009;249:809–21. https://doi.org/10.1016/j.desal.2009.04.011

[6]Tedesco M, Hamelers H, Biesheuvel P. Nernst-Planck transport theory for (reverse) electrodialysis: III. Optimal membrane thickness for enhanced process performance. J Membr Sci 2018;565:480–7. https://doi.org/https://doi.org/10.1016/j.memsci.2018.07.090.

[7]Azad H, Mohsennia M. A novel free-standing polyvinyl butyral-polyacrylonitrile/ZnAl-layered double hydroxide nanocomposite membrane for enhanced heavy metal removal from wastewater. J Membr Sci 2020;615:118487. https://doi.org/https://doi.org/10.1016/j.memsci.2020.11848.

[8]Ghasemi M, Sedighi M, Usefi MMB. A comprehensive review on membranes in microbial desalination cells; processes, utilization, and challenges. Int J Energy Res 2022;46:14716–39. https://doi.org/https://doi.org/10.1002/er.8265.

[9]Mehdizadeh S, Yasukawa M, Kuno M, Kawabata Y, Higa M. Evaluation of energy harvesting from discharged solutions in a salt production plant by reverse electrodialysis (RED). Desalination 2019;467:95–102. https://doi.org/10.1016/j.desal.2019.04.007

[10] Jang J, Kang Y, Han J-H, Jang K, Kim C-M, Kim IS. Developments and future prospects of reverse electrodialysis for salinity gradient power generation: Influence of ion exchange membranes and electrodes. Desalination 2020;491:114540. https://doi.org/10.1016/j.desal.2020.114540

[11] Chen T-H, Chen Y-A, Tsai S-W, Wang D-M, Hou C-H. Development of an integrated capacitive-electrodialysis process (CapED) for continuous, low-energy electrochemical deionization. Sep Purif Technol 2021;274:119063. https://doi.org/https://doi.org/10.1016/j.seppur.2021.119063.

[12] Dammak L, Fouilloux J, Bdiri M, Larchet C, Renard E, Baklouti L, Sarapulova V, Kozmai A, Pismenskaya N. A review on ion-exchange membrane fouling during the electrodialysis process in

the food industry, part 1: Types, effects, characterization methods, fouling mechanisms and interactions. Membranes 2021;11:789. https://doi.org/https://doi.org/10.3390/membranes11100789.

[13] Mohammadi R, Tang W, Sillanpää M. A systematic review and statistical analysis of nutrient recovery from municipal wastewater by electrodialysis. Desalination 2021;498:114626. https://doi.org/10.1016/j.desal.2020.114626.

[14] Hosseini S, Usefi MB, Habibi M, Parvizian F, Van der Bruggen B, Ahmadi A, Nemati M. Fabrication of mixed matrix anion exchange membrane decorated with polyaniline nanoparticles to chloride and sulfate ions removal from water. Ionics 2019;25:6135–45. https://doi.org/https://doi.org/10.1007/s11581-019-03151-w.

[15] Azad H, Mohsennia M, Cheng C, Amini A. Cross-linked poly (vinyl butyral)/amine-functionalized polyacrylonitrile adsorptive membrane nano-composited with CeO2 nanoparticles for simultaneous aqueous removal of heavy metals and cefotaxime. Chem Eng J 2022;435:134849. https://doi.org/10.1016/j.cej.2022.134849.

[16] Chakraborty I, Das S, Dubey B, Ghangrekar M. Novel low cost proton exchange membrane made from sulphonated biochar for application in microbial fuel cells. Mater Chem Phys 2020;239:122025. https://doi.org/https://doi.org/10.1016/j.matchemphys.2019.122025.

[17] Pendergast MM, Hoek EM. A review of water treatment membrane nanotechnologies. Energy Environ Sci 2011;4:1946–71. https://doi.org/DOI%09https://doi.org/10.1039/C0EE00541J.

[18] Alabi A, AlHajaj A, Cseri L, Szekely G, Budd P, Zou L. Review of nanomaterials-assisted ion exchange membranes for electromembrane desalination. Npj Clean Water 2018;1:10. https://doi.org/https://doi.org/10.1038/s41545-018-0009-7.

[19] Mishra JR, Samal SK, Mohanty S, Nayak SK. Polyvinylidene fluoride (PVDF)/Ag@ TiO2 nanocomposite membrane with enhanced fouling resistance and antibacterial performance. Mater Chem Phys 2021;268:124723. https://doi.org/https://doi.org/10.1016/j.matchemphys.2021.124723.

[20] Nasrollahi N, Aber S, Vatanpour V, Mahmoodi NM. Development of hydrophilic microporous PES ultrafiltration membrane containing CuO nanoparticles with improved antifouling and separation performance. Mater Chem Phys 2019;222:338–50. https://doi.org/https://doi.org/10.1016/j.matchemphys.2018.10.032.

[21] Sahoo NG, Rana S, Cho JW, Li L, Chan SH. Polymer nanocomposites based on functionalized carbon nanotubes. Prog Polym Sci 2010;35:837–67. https://doi.org/10.1016/j.progpolymsci.2010.03.002.

[22] Spitalsky Z, Tasis D, Papagelis K, Galiotis C. Carbon nanotube–polymer composites: chemistry, processing, mechanical and electrical properties. Prog Polym Sci 2010;35:357–401. https://doi.org/10.1016/j.progpolymsci.2009.09.003.

[23] Jhaveri JH, Murthy Z. A comprehensive review on anti-fouling nanocomposite membranes for pressure driven membrane separation processes.

Desalination 2016;379:137–54. https://doi.org/10.1016/j.desal.2015.11.009

[24] Fernandez-Gonzalez C, Zhang B, Dominguez-Ramos A, Ibañez R, Irabien A, Chen Y. Enhancing fouling resistance of polyethylene anion exchange membranes using carbon nanotubes and iron oxide nanoparticles. Desalination 2017;411:19–27. https://doi.org/10.1016/j.desal.2017.02.00.

[25] Liu Y, Chen J, Chen R, Zhou T, Ke C, Chen X. Effects of multi-walled carbon nanotubes on bipolar membrane properties. Mater Chem Phys 2018;203:259–65. https://doi.org/10.1016/j.matchemphys.2017.09.068.

[26] Jaroszek H, Dydo P. Potassium nitrate synthesis by electrodialysis-metathesis: The effect of membrane type. J Membr Sci 2018;549:28–37. https://doi.org/https://doi.org/10.1016/j.memsci.2017.11.062.

[27] Zhang X, Han X, Yan X, Chen X, Jin Z, Hu X. Continuous synthesis of high purity KNO3 through electrodialysis metathesis. Sep Purif Technol 2019;222:85–91. https://doi.org/https://doi.org/10.1016/j.seppur.2019.04.027.

[28] Wei X, Gao W, Wang Y, Wu K, Xu T. A green and economical method for preparing lithium hydroxide from lithium phosphate. Sep Purif Technol 2022;280:119909. https://doi.org/https://doi.org/10.1021/acs.iecr.1c04556.

[29] Han X, Yan X, Wang X, Ran J, Wu C, Zhang X. Preparation of chloride-free potash fertilizers by electrodialysis metathesis. Sep Purif Technol 2018;191:144–52. https://doi.org/https://doi.org/10.1016/j.seppur.2017.09.022.

[30] Hosseini S, Koranian P, Gholami A, Madaeni S, Moghadassi A, Sakinejad P, Khodabakhshi A. Fabrication of mixed matrix heterogeneous ion exchange membrane by multiwalled carbon nanotubes: Electrochemical characterization and transport properties of mono and bivalent cations. Desalination 2013;329:62–7. https://doi.org/10.1016/j.desal.2013.09.007

[31] Zendehnam A, Mokhtari S, Hosseini S, Rabieyan M. Fabrication of novel heterogeneous cation exchange membrane by use of synthesized carbon nanotubes-co-copper nanolayer composite nanoparticles: Characterization, performance in desalination. Desalination 2014;347:86–93. https://doi.org/10.1016/j.desal.2014.05.041

[32] Hosseini S, Jeddi F, Nemati M, Madaeni S, Moghadassi A. Electrodialysis heterogeneous anion exchange membrane modified by PANI/MWCNT composite nanoparticles: Preparation, characterization and ionic transport property in desalination. Desalination 2014;341:107–14. https://doi.org/10.1016/j.desal.2014.03.001

[33] Chan W-F, Chen H, Surapathi A, Taylor MG, Shao X, Marand E, Johnson JK. Zwitterion functionalized carbon nanotube/polyamide nanocomposite membranes for water desalination. Acs Nano 2013;7:5308–19. https://doi.org/https://doi.org/10.1021/nn4011494.

[34] Hosseini S, Madaeni S, Heidari A, Amirimehr A. Preparation and characterization of ion-selective polyvinyl chloride based heterogeneous cation exchange membrane modified by magnetic iron–nickel oxide nanoparticles. Desalination 2012;284:191–9. https://doi.org/10.1016/j.desal.2011.08.057

[35] Barros KS, Scarazzato T, Pérez-Herranz V, Espinosa DCR. Treatment of

cyanide-free wastewater from brass electrodeposition with edta by electrodialysis: Evaluation of underlimiting and overlimiting operations. Membranes 2020;10:69. https://doi.org/https://doi.org/10.3390/membranes10040069.

[36] Ferreira AR, Couto N, Guedes P, Pinto J, Mateus EP, Ribeiro AB. Electrodialytic 2-compartment cells for emerging organic contaminants removal from effluent. J Hazard Mater 2018;358:467–74. https://doi.org/https://doi.org/10.1016/j.jhazmat.2018.04.066.

[37] La Cerva M, Gurreri L, Tedesco M, Cipollina A, Ciofalo M, Tamburini A, Micale G. Determination of limiting current density and current efficiency in electrodialysis units. Desalination 2018;445:138–48. https://doi.org/10.1016/j.desal.2018.02.020

[38] Yan K-K, Jiao L, Lin S, Ji X, Lu Y, Zhang L. Superhydrophobic electrospun nanofiber membrane coated by carbon nanotubes network for membrane distillation. Desalination 2018;437:26–33. https://doi.org/10.22078/jpst.2017.2577.1441.

[39] Hosseini SM, Alibakhshi H, Khodabakhshi AR, Nemati M. Enhancing electrochemical performance of heterogeneous cation exchange membranes by using super activated carbon nanoparticles. J Pet Sci Technol 2018;8:14–29. https://doi.org/10.22078/jpst.2017.2577.1441.

[40] Zhao Y, Duan L. Research on Measuring Pure Membrane Electrical Resistance under the Effects of Salinity Gradients and Diffusion Boundary Layer and Double Layer Resistances. Membranes 2022;12:816. https://doi.org/https://doi.org/10.3390/membranes12080816.

[41] Sharma PP, Gahlot S, Rajput A, Patidar R, Kulshrestha V. Efficient and cost effective way for the conversion of potassium nitrate from potassium chloride using electrodialysis. ACS Sustain Chem Eng 2016;4:3220–7. https://doi.org/https://doi.org/10.1021/acssuschemeng.6b00248.

[42] Zahakifar F, Keshtkar A, Souderjani EZ, Moosavian M. Use of response surface methodology for optimization of thorium (IV) removal from aqueous solutions by electrodeionization (EDI). Prog Nucl Energy 2020;124:103335. https://doi.org/https://doi.org/10.1016/j.pnucene.2020.103335.

[43] Chang J, Duan F, Cao H, Tang K, Su C, Li Y. Superiority of a novel flow-electrode capacitive deionization (FCDI) based on a battery material at high applied voltage. Desalination 2019;468:114080. https://doi.org/10.1016/j.desal.2019.114080.

[44] Phuoc NM, Tran NAT, Khoi TM, Jung HB, Ahn W, Jung E, Yoo C-Y, Kang HS, Cho Y. ZIF-67 metal-organic frameworks and CNTs-derived nanoporous carbon structures as novel electrodes for flow-electrode capacitive deionization. Sep Purif Technol 2021;277:119466. https://doi.org/https://doi.org/10.1016/j.seppur.2021.119466.

[45] Al-Amshawee SKA, Yunus MYBM. Electrodialysis membrane with concentration polarization–a review. Chem Eng Res Des 2024;201:645–78. https://doi.org/https://doi.org/10.1016/j.cherd.2023.10.060.

[46] Geise GM, Curtis AJ, Hatzell MC, Hickner MA, Logan BE. Salt concentration differences alter membrane resistance in reverse electrodialysis stacks. Environ Sci

Technol Lett 2014;1:36–9. https://doi.org/https://doi.org/10.1021/ez400719.

[47] Jia YW, Chen GQ, Kentish SE. Investigating the effect of temperature and concentration on the performance of reverse electrodialysis systems. Desalination 2024;592:118184. https://doi.org/10.1016/j.desal.2024.118184.

[48] Avci AH, Messana DA, Santoro S, Tufa RA, Curcio E, Di Profio G, Fontananova E. Energy harvesting from brines by reverse electrodialysis using nafion membranes. Membranes 2020;10:168. https://doi.org/https://doi.org/10.3390/membranes10080168.

[49] Ebrahimi M, Van der Bruggen B, Askari M, Nemati M. Improving electrochemical properties of cation exchange membranes by using activated carbon-co-chitosan composite nanoparticles in water deionization. Ionics 2019;25:1199–214. https://doi.org/https://doi.org/10.1007/s11581-018-2724-y.

[50] Fan H, Huang Y, Yip NY. Advancing the conductivity-permselectivity tradeoff of electrodialysis ion-exchange membranes with sulfonated CNT nanocomposites. J Membr Sci 2020;610:118259. https://doi.org/https://doi.org/10.1016/j.memsci.2020.118259.

[51] Zhou R, Rana D, Matsuura T, Lan CQ. Effects of multi-walled carbon nanotubes (MWCNTs) and integrated MWCNTs/SiO2 nano-additives on PVDF polymeric membranes for vacuum membrane distillation. Sep Purif Technol 2019;217:154–63. https://doi.org/https://doi.org/10.1016/j.seppur.2019.02.013.

[52] Moghadassi A, Koranian P, Hosseini S, Askari M, Madaeni S. Surface modification of heterogeneous cation exchange membrane through simultaneous using polymerization of PAA and multi walled carbon nano tubes. J Ind Eng Chem 2014;20:2710–8. https://doi.org/10.1016/j.jiec.2013.10.059.

[53] Bagheripour E, Moghadassi A, Hosseini SM. Preparation of mixed matrix PES-based nanofiltration membrane filled with PANI-co-MWCNT composite nanoparticles. Korean J Chem Eng 2016;33:1462–71. https://doi.org/https://doi.org/10.1007/s11814-015-0257-x.